PCCP

Physical Chemistry Chemical Physics

www.rsc.org/pccp

Volume 15 | Number 28 | 28 July 2013 | Pages 11589–11968

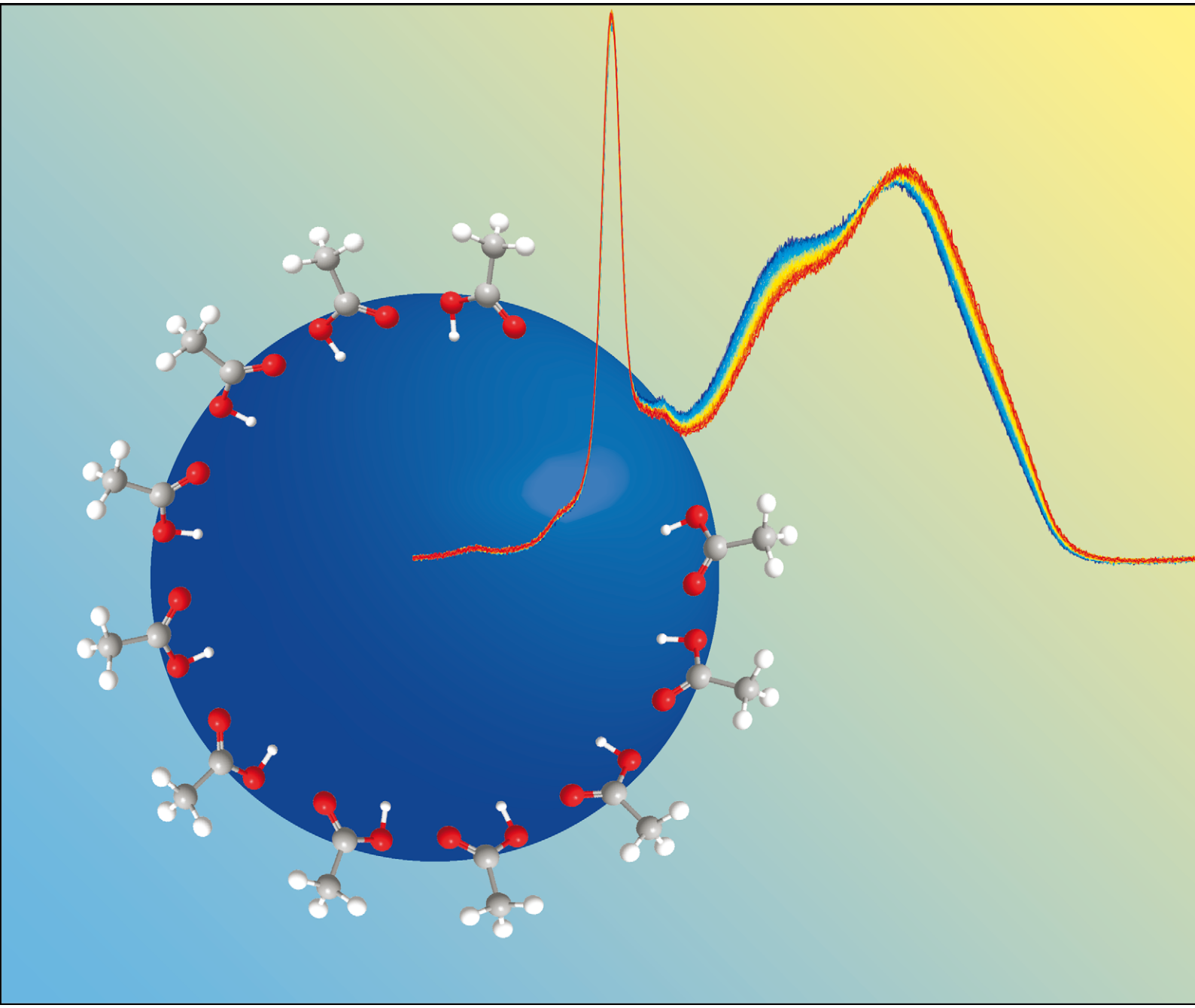

ISSN 1463-9076

PAPER

Richard J. Saykally, Ronald C. Cohen *et al.*

Evaporation kinetics of aqueous acetic acid droplets: effects of soluble organic aerosol components on the mechanism of water evaporation

1463-9076(2013)15:28;1-K

PCCP

RSC Publishing

PAPER

Evaporation kinetics of aqueous acetic acid droplets: effects of soluble organic aerosol components on the mechanism of water evaporation

Cite this: *Phys. Chem. Chem. Phys.*, 2013, **15**, 11634

Kaitlin C. Duffey,[ab] Orion Shih,[ab] Nolan L. Wong,[a] Walter S. Drisdell,[c] Richard J. Saykally*[ab] and Ronald C. Cohen*[ad]

Received 15th March 2013,
Accepted 3rd May 2013

DOI: 10.1039/c3cp51148k

www.rsc.org/pccp

The presence of organic surfactants in atmospheric aerosol may lead to a depression of cloud droplet growth and evaporation rates affecting the radiative properties and lifetime of clouds. Both the magnitude and mechanism of this effect, however, remain poorly constrained. We have used Raman thermometry measurements of freely evaporating micro-droplets to determine evaporation coefficients for several concentrations of acetic acid, which is ubiquitous in atmospheric aerosol and has been shown to adsorb strongly to the air–water interface. We find no suppression of the evaporation kinetics over the concentration range studied (1–5 M). The evaporation coefficient determined for 2 M acetic acid is 0.53 ± 0.12, indistinguishable from that of pure water (0.62 ± 0.09).

Introduction

Understanding the mechanism of water evaporation (condensation) from (onto) the surfaces of micron-sized droplets in our atmosphere is important for our ability to predict cloud droplet growth rates and thus to determine the effect of aerosol composition on cloud properties.[1–5] Despite decades of study, uncertainty remains as to the rate of evaporation and condensation of pure water,[6–9] the magnitude and mechanism by which surfactants impede evaporation and condensation,[10–13] and the importance of these kinetic effects to cloud properties.[14–16]

The kinetics of evaporation and condensation are reflected in the evaporation (or mass accommodation) coefficient. This coefficient is the empirically-determined ratio of the observed flux of molecules evaporating from (or condensing onto) a liquid surface to the maximum flux permitted by gas kinetic theory. The Hertz-Knudsen equation describes the flux through the interface between a liquid and its vapor. For condensation,

$$J_c = \alpha \frac{p}{\sqrt{2\pi mkT}} \quad (1)$$

where J_c is the flux of molecules condensing into the liquid, in molecules m^{-2} s^{-1}, p, T, and m are the pressure, temperature, and molecular mass of the vapor, k is the Boltzmann constant, and α is the mass accommodation coefficient. An analogous expression may be written for evaporation:

$$J_e = \gamma \frac{p_{sat}}{\sqrt{2\pi mkT_{surf}}} \quad (2)$$

Here J_e is the evaporative flux, p_{sat} is the saturation vapor pressure of the liquid, and T_{surf} is the temperature of the molecules at the liquid surface. Microscopic reversibility requires that the mass accommodation and evaporation coefficients for a system be equivalent (for simplicity, we will henceforth refer only to evaporation, but this equivalence should be kept in mind). An evaporation coefficient smaller than unity indicates a kinetic barrier to the evaporation process; *i.e.*, evaporating molecules must pass through a transition state involving an energetic barrier and/or a specific spatial orientation. Experimental values of γ can, in combination with simulations, yield insight into the molecular mechanism of evaporation.

Measurements of γ are notoriously challenging and reported values for pure water vary by orders of magnitude depending on the experimental technique used.[6,8,17] Marek and Straub[6] provide an extensive review of measurements made over the past century, noting that surface impurities are the likely origin of γ values below 0.1 determined from experiments on stagnant surfaces. A more recent review by Miles *et al.*[8] addresses uncertainties in thermophysical parameters used to determine

[a] *Department of Chemistry, University of California, Berkeley, CA 94720, USA. E-mail: saykally@berkeley.edu, rccohen@berkeley.edu*
[b] *Chemical Sciences Division, Lawrence Berkeley National Laboratory, One Cyclotron Road, Berkeley, CA 94720, USA*
[c] *Materials Science Division, Lawrence Berkeley National Laboratory, USA*
[d] *Department of Earth and Planetary Science, University of California, Berkeley, USA*

γ from cloud chamber, flow tube, and single-particle levitation studies. They conclude that the coefficient for pure water is above 0.5, but that uncertainties in water vapor supersaturation and diffusion through the gas phase make it impossible to obtain a more precise value in experiments conducted near liquid–vapor equilibrium. Our experimental technique, in which we measure the temperature of micron-sized droplets as they evaporate freely into vacuum, allows for a relatively precise determination of γ. This technique yields a coefficient of 0.62 ± 0.09 for pure water, indicating that there is a small kinetic barrier to evaporation.[7]

No kinetic barrier has been observed in molecular dynamics simulations.[18–21] Most theoretical studies of evaporation and condensation kinetics have focused on mass accommodation, as evaporation is an extremely rare event in simulations (one water molecule evaporates per 10 nm^2 per 10 ns). A recent study by Varilly and Chandler,[9] in which transition path sampling was used to harvest and analyze simulated evaporation trajectories, found that the evaporation process is well-described as diffusion out of a potential energy well, consistent with an evaporation coefficient of unity. The difference between our experimental results for pure water and those of theoretical studies remains unresolved. Interestingly, Varilly and Chandler also found that evaporation events occur more often when the mean curvature of the liquid surface beneath the evaporating molecule is negative, evidence that collective motions of liquid water molecules play a role in the evaporation process.

Examination of the effects of solutes on evaporation kinetics can yield additional insight into the molecular mechanism of water evaporation. The evaporation coefficient of 4 M sodium perchlorate was determined using our technique to be 25% lower than that of pure water, indicating that the interaction of surface water molecules with the highly surface-active perchlorate anion decreases their likelihood of evaporating.[22] The explanation that has been suggested for this observed decrease is that water–ion interactions hinder the librational motions of the water molecules, which have been found to be central in transition state theory studies of evaporation.[23]

In addition to providing mechanistic information, the evaporation coefficient is a useful parameter in cloud microphysical models. These models often assume that evaporation is much faster than molecular transport through the gas phase, so that micron-sized droplets quickly reach equilibrium with their immediate surroundings and droplet evolution is determined solely by thermodynamic conditions. This assumption is valid if the evaporation coefficient is greater than 0.1.[2,24] Because cloud droplets form by the uptake of water onto chemically-complex aerosol particles, they can, at least in the early phases of droplet growth, contain high concentrations of soluble surfactants and can also be coated with fatty acid films.[25–30] Molecular dynamics simulations show that surfactants can depress the evaporation coefficient by several orders of magnitude,[12] potentially causing cloud models to under-predict cloud droplet numbers and leading to inaccuracies in modelled cloud height, reflectivity, and lifetime.[2,24,31] Discrepancies between modelled and measured cloud condensation nucleation (CCN) activity in field studies have provided evidence of kinetically-limited droplet growth in the atmosphere.[3,15] However, in a recent analysis of global CCN data, Raatikainen *et al.* (2013) suggest that the effective mass accommodation coefficient of ambient aerosol is greater than 0.1 in all regions of the globe, and hence that cloud properties can be accurately predicted using the current equilibrium models.[16]

Recently, Davies *et al.*[13] measured rates of water evaporation through surfactant monolayers by monitoring the size evolution of droplets suspended in an electrodynamic balance.[4,13] They observed a transition from thermodynamically-limited to kinetically-limited evaporation when the droplet became small enough (and its surfactant concentration high enough) that a densely-packed solid film formed on its surface. The evaporation coefficient for solid-film-coated droplets was observed to decrease with surfactant chain length from 2.4×10^{-3} for dodecanol (C_{12}) to 1.7×10^{-5} for heptadecanol (C_{17}).[13] In contrast, kinetically-limited evaporation was never observed for droplets coated with the soluble C_{12} surfactant sodium dodecyl sulfate.[4] The mechanistic interpretation of these results is that the Van der Waals interactions between hydrophobic moieties oriented parallel to the droplet surface form a seal that prevents water molecules from escaping, drastically impeding evaporation rates. Such highly-ordered solid films are not likely to be prevalent in the atmosphere; hence the authors argued that kinetic limitation of cloud droplet evolution is unlikely.[13] One drawback to the approach of Davies *et al.* is that it cannot be used to distinguish γ values greater than 0.05 due to uncertainties associated with mass and heat transport through the gas phase. A less-drastic effect of surfactants on the kinetics of evaporation, *e.g.*, through changes to the hydrogen bonding environment or larger-scale collective motions of interfacial water molecules, would be undetectable using this technique.

Here we present the application of our free evaporation method to determine γ for varying concentrations of acetic acid in order to investigate the relationship between surface composition and evaporation. Although miscible with water, acetic acid behaves as a surfactant, causing surface tension to decrease by 30% over a concentration range of 0 to 10%. This leads to a calculated surface concentration of 60% for a 10% acetic acid solution.[32] Sum frequency generation (SFG) spectra show that the vibrational modes of interfacial water molecules change significantly upon the addition of small amounts of acetic acid (the hydrogen bonded and free OH stretching bands present in the pure water spectrum are absent in the spectrum of 1.6% acetic acid solution), providing experimental evidence that acetic acid adsorbs to the interface and changes its hydrogen bond structure.[33]

By comparing the kinetic effects of acetic acid (a small, soluble carboxylic acid) with those of similarly surface-active perchlorate (a strongly hydrated anion) and insoluble long-chain fatty acids, we hope to gain further insight into the mechanisms by which surfactants perturb evaporation. The evaporation rate of water in the presence of small carboxylic acids is pertinent to our understanding of aerosol microphysics. The suppression of cloud droplet evolution *via* the formation of impermeable fatty acid monolayers has been demonstrated to

be unlikely;[13] however, soluble carboxylic acids such as acetic and oxalic acids are ubiquitous in atmospheric aerosol and their concentrations can be high in growing cloud droplets.[30] The disruption of interfacial structure by these species is another possible mechanism by which evaporation may be impeded in the atmosphere.

Experimental

Sample preparation

Acetic acid solutions were prepared volumetrically using glacial acetic acid (EMD chemicals, >99.7% purity) and filtered, deionized water (Millipore, 18 MΩ).

Raman thermometry measurements

Our measurements are made using the experimental setup described by Smith *et al.*[7,22,34,35] A train of uniformly-sized droplets is generated by pumping a liquid sample through a tapered fused silica nozzle (New Objective) attached to a vibrating piezo-electric. The droplet train is directed into a vacuum chamber evacuated to 10^{-4} torr. The droplets are small enough (7–10 μ in radius) that evaporating molecules undergo less than one gas-phase collision on average, minimizing the possibility of re-condensation onto the droplet surface. The assumption of free evaporation is considered in detail by Smith *et al.*[7]

Raman spectra of the droplets are obtained at various distances from the nozzle by adjusting the position of the droplet train with respect to the focal point of an argon ion laser beam (514 nm) in the center of the chamber. Scattered light is collected at 90° to the incident beam and directed into a spectrophotometer (Fig. 1). The average droplet temperature is determined from the shape of the OH stretching feature using the calibration method described previously.[7,36] Fig. 2a shows spectra of 2 M acetic acid collected in a cuvette over a range of temperatures measured with a thermocouple. The associated calibration curve is shown in Fig. 2b.

Measured droplet temperatures are plotted as a function of residence time in vacuum (determined from the linear velocity of the droplets) and the data are compared to an evaporative cooling model, discussed below, in which γ is the only adjustable parameter.

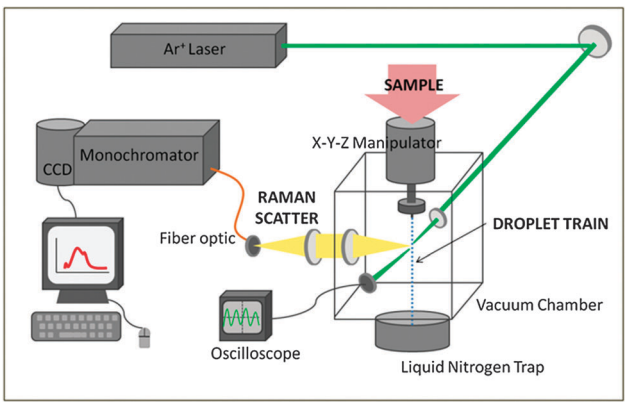

Fig. 1 Experimental setup.

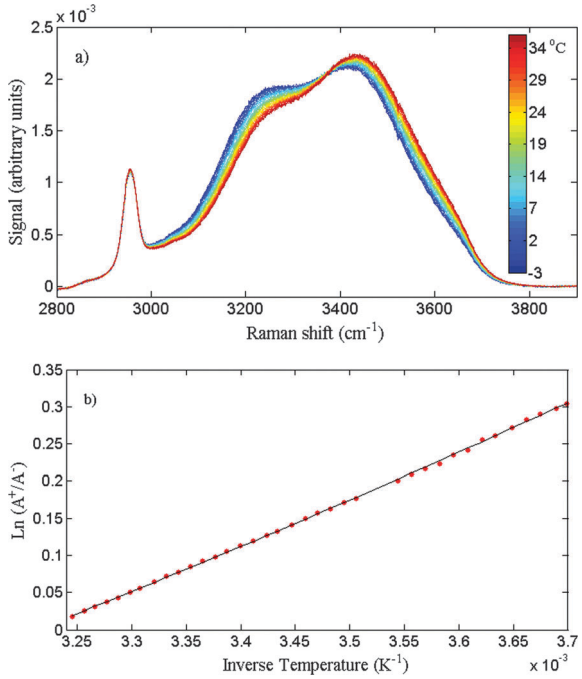

Fig. 2 (a) Raman spectra of 2 M acetic acid collected in a cuvette at various temperatures. (b) Corresponding calibration curve: natural logarithm of the ratio of integrated peak areas above and below 3450 cm^{-1} *vs.* inverse temperature. The black dashed line is the quadratic fit used to determine droplet temperatures.

It should be noted that the droplets in our experiment become supercooled to temperatures as low as 250 K and that we are only able to obtain calibration spectra above the freezing point of the solution. We therefore apply a quadratic fit to the calibration data and extend this fit into the supercooled regime to determine experimental droplet temperatures. Our assumption that the temperature dependence of the Raman spectrum does not change below the freezing point is supported by recent measurements of optically-levitated supercooled water droplets in a temperature-controlled chamber.[37]

The feature at 2960 cm^{-1} in Fig. 2a is due to the OH stretch of acetic acid. This feature shows no temperature dependence and its intensity is proportional to acetic acid concentration. Because it overlaps with the OH stretching band of water, this feature is included in the integrated peak area used for the temperature calibration. Although the concentration of acetic acid likely increases slightly as the droplets evaporate due to the higher vapor pressure of water, this effect is minimal and the intensity of the 2960 cm^{-1} peak does not change sufficiently over the timescale of the experiment to bias our measured temperatures.

Cooling model

In order to determine the evaporation coefficient from our data, we numerically describe the cooling rate of a spherical droplet undergoing evaporation without condensation. Heat transfer

within the droplet is assumed to occur *via* conduction only, and the droplet is divided into spherical shells, allowing for a temperature gradient to form within the droplet and heat to flow from the interior to the surface. The surface of our model droplet cools at a rate proportional to the evaporative flux

$$\frac{dT}{dt} = -\frac{\gamma p_{sat}}{\sqrt{2\pi mkT}} \frac{\Delta H_{vap}}{C_p} \frac{3r_0^2}{(r_0^3 - r_1^3)\rho} \quad (3)$$

where ΔH_{vap} is the enthalpy of vaporization of the evaporating water molecules, C_p and ρ are the heat capacity and density of the surface shell, and r is the radius (subscripts 0 and 1 indicate the outermost shell and the first sub-shell, respectively). Heat is then conducted outward from each sub-shell of the droplet:

$$\frac{dQ}{dt} = -\kappa A \frac{dT}{dr} \quad (4)$$

Here Q is heat, κ is thermal conductivity, and A is the surface area of the sub-shell. Eqn (3) and (4) are numerically integrated and the physical parameters are adjusted at each time step so they are temperature-dependent.

To be complete in describing an acetic acid–water mixture, eqn (3) should include a separate term for the heat removed from the droplet surface by evaporating acetic acid molecules. However, the maximum acetic acid concentration studied here was 5 M (x = 0.011), for which the ratio

$$\frac{p_{sat,w}\Delta H_{vap,w}\sqrt{m_a}}{p_{sat,a}\Delta H_{vap,a}\sqrt{m_w}}$$

(the subscripts a and w indicate acetic acid and water, respectively, and the vapor pressure and enthalpy values are those reported for vapor–liquid equilibrium of an acetic acid–water mixture at 298 K) is sufficiently large that the cooling contribution from acetic acid evaporation may be ignored.[38] Density, heat capacity, and thermal conductivity of acetic acid solutions were obtained from reported literature values.[38–41] The vapor pressure of water was calculated using an empirical temperature-dependent equation for pure water[42] and scaled by the activity.[43] The enthalpy of vaporization was assumed to be equal to that of pure water; this assumption was validated by examining the temperature dependence of reported equilibrium water vapor pressures of equilibrated acetic acid–water mixtures. Since evaporation is occurring into a vacuum, the pressure–volume work, equal to kT, is subtracted from the enthalpy.

Results and discussion

Four cooling curves were obtained for 2 M acetic acid (mole fraction, x = 0.04), with droplet radii ranging from 7–9 microns. The average evaporation coefficient determined from this set of experiments was 0.53 ± 0.12 (95% confidence interval). Fig. 3 shows the cooling curve from a single experiment with the output of our cooling model. The sensitivity of the cooling model to each of the thermodynamic parameters was tested. A 10% error in enthalpy of vaporization, heat capacity, thermal conductivity, vapor pressure, or density induces an error of less than 0.1 in the evaporation coefficient; the uncertainty associated with the temperature determination prevents us from attaining greater than 0.1 precision in the evaporation coefficient for each individual cooling curve.

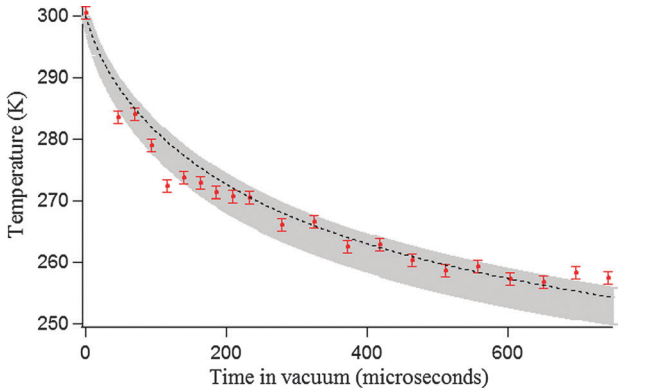

Fig. 3 Temperature *vs.* time for a 2 M acetic acid solution. Raman thermometry measurements (red), cooling model output for γ = 0.45 (black), and the 95% confidence interval obtained by repeating the experiment 4 times (shaded region).

Our cooling model assumes uniform droplet composition; however, acetic acid enrichment at the droplet surface may produce gradients in the thermophysical parameters near the interface. In order to test the effect of an enhanced surface concentration on the cooling curve, we modified the model by allowing the outermost 5 nm shell of the droplet to have heat capacity, density, and thermal conductivity values equal to those of a 50% acetic acid solution (the surface concentration predicted for 2 M acetic acid[32]). This resulted in a decrease in the observed evaporation coefficient of roughly 0.1, which is within our experimental uncertainty.

The 95% confidence interval of our measured γ for 2 M acetic acid overlaps with that of pure water. Cooling curves were obtained for a variety of concentrations ranging from 1 M (x = 0.02) to 5 M (x = 0.11). Fig. 4 shows the evaporation coefficients for all experiments plotted against acetic acid mole fraction. There is no apparent dependence of γ on acetic acid mole fraction, nor is there a statistically-significant reduction in the coefficient compared to that of pure water for even the highest concentration studied.

This result supports the conclusion of Davies *et al.*[13] that a tightly-packed hydrocarbon layer is required to cause γ to decrease by more than an order of magnitude, with increased carbon chain length causing a greater reduction. The hydrophobic groups of long-chain surfactants are tilted with respect to the surface, allowing for strong Van der Waals interactions between adjacent surfactant molecules and forming a physical barrier to evaporation.[44] Polarization-dependent SFG spectra indicate that interfacial acetic acid molecules are oriented upright, with the methyl group directed away from the aqueous phase.[32] Hence a monolayer of acetic acid molecules would not be expected to create a hydrophobic seal.

The lack of a smaller but observable change in γ with increasing acetic acid concentration is surprising, however, in the context of our previous studies, which suggested that solutes adsorbed to the liquid surface impact the kinetics of

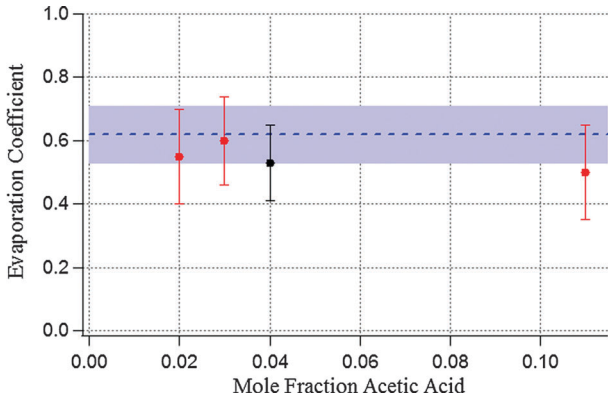

Fig. 4 Evaporation coefficient *vs.* acetic acid mole fraction. Red points are single experiments with error bars representing the γ range needed to encompass all points on the cooling curve. The black point is 2 M acetic acid with error bars representing the 95% confidence interval of the best γ fit for 4 experiments.

evaporation by changing the hydrogen bonding environment of surface water molecules. Surface tension measurements and spectroscopic studies indicate that acetic acid has a higher surface affinity than does sodium perchlorate, which at a concentration of 4 M (x = 0.07) decreases the evaporation coefficient by 20% compared to that of pure water. The microscopic reasons for this difference in behavior are unclear. Drisdell *et al.*[22] speculated that the surface water molecules interacting directly with perchlorate anions were less likely to evaporate due to hindered librational motions. The hydration number for acetic acid is 2[45] while that for perchlorate is 3.8;[46] hence if direct solute–water interactions are responsible for the decrease in evaporation kinetics, a higher surface mole fraction of acetic acid would be required to cause the same 25% decrease in the evaporation coefficient. It is possible that the acetic acid mole fractions studied here were simply too low to produce a distinguishable change. Uncertainties in the surface-to-bulk acetic acid concentration gradient in our droplets, as well as a lack of knowledge about the molecular structure and pH of the aqueous acetic acid interface[47,48] prevent us from speculating further here; more experimental and theoretical work is needed to understand the connections between interfacial structure and evaporation.

Conclusions

We have measured evaporation rates of micron-sized water droplets containing several different concentrations of acetic acid. For 2 M acetic acid, we have determined the evaporation coefficient to be 0.53 ± 0.12, which is indistinguishable from the previously-determined coefficient for pure water. This suggests that the presence of acetic acid molecules at the air–water interface does not impact the kinetics of water evaporation as does the presence of perchlorate anions. Simulations of the molecular structure of the air–aqueous acetic acid interface are needed to explore the microscopic factors underlying these observations.

Our results are in agreement with recent studies of surfactant effects on evaporation, which have indicated that a complete monolayer of an insoluble surfactant is required to impede the evaporation of water sufficiently for cloud droplet evolution to be limited by kinetics rather than thermodynamics.

Acknowledgements

The authors thank Dr. Patrick Varilly for insightful discussions about evaporation and for his input regarding our temperature calibrations and cooling model. We also thank Frank Liu and Michael Angell for their assistance in collecting data. This work was supported by National Science Foundation Grant ATM 0639847 and the Director, Office of Science, Office of Basic Energy Sciences, of the U.S. Department of Energy under Contract DE-AC02-05CH11231.

References

1 P. Y. Chuang, R. J. Charlson and J. H. Seinfeld, *Nature*, 1997, **390**, 594–596.
2 G. Feingold and P. Y. Chuang, *J. Atmos. Sci.*, 2002, **59**, 2006–2018.
3 C. R. Ruehl, P. Y. Chuang and A. Nenes, *Atmos. Chem. Phys.*, 2008, **8**, 1043–1055.
4 J. F. Davies, A. E. Haddrell, R. E. H. Miles, C. R. Bull and J. P. Reid, *J. Phys. Chem. A*, 2012, **116**, 10987–10998.
5 D. L. Bones, J. P. Reid, D. M. Lienhard and U. K. Krieger, *Proc. Natl. Acad. Sci. U. S. A.*, 2012, **109**, 11613–11618.
6 R. Marek and J. Straub, *Int. J. Heat Mass Transfer*, 2001, **44**, 39–53.
7 J. D. Smith, C. D. Cappa, W. S. Drisdell, R. C. Cohen and R. J. Saykally, *J. Am. Chem. Soc.*, 2006, **128**, 12892–12898.
8 R. E. H. Miles, J. P. Reid and I. Riipinen, *J. Phys. Chem. A*, 2012, **116**, 10810–10825.
9 P. Varilly and D. Chandler, *J. Phys. Chem. B*, 2013, **117**, 1419–1428.
10 G. T. Barnes, *Adv. Colloid Interface Sci.*, 1986, **25**, 89–200.
11 A. Gilde, N. Siladke and C. P. Lawrence, *J. Phys. Chem. A*, 2009, **113**, 8586–8590.
12 S. Takahama and L. M. Russell, *J. Geophys. Res.: Atmos.*, 2011, **116**, D02203.
13 J. F. Davies, R. E. H. Miles, A. E. Haddrell and J. P. Reid, *Proc. Natl. Acad. Sci. U. S. A.*, 2013, in press.
14 P. S. Gill, T. E. Graedel and C. J. Weschler, *Rev. Geophys.*, 1983, **21**, 903–920.
15 N. C. Shantz, J. R. Pierce, R. Y.-W. Chang, A. Vlasenko, I. Riipinen, S. Sjostedt, J. G. Slowik, A. Wiebe, J. Liggio, J. P. D. Abbatt and W. R. Leaitch, *Atmos. Environ.*, 2012, **47**, 389–398.
16 T. Raatikainen, *et al.*, *Proc. Natl. Acad. Sci. U. S. A.*, 2013, **110**, 3760–3764.
17 C. E. Kolb, R. A. Cox, J. P. D. Abbatt, M. Ammann, E. J. Davis, D. J. Donaldson, B. C. Garrett, C. George, P. T. Griffiths, D. R. Hanson, M. Kulmala, G. McFiggans, U. Poeschl, I. Riipinen, M. J. Rossi, Y. Rudich, P. E. Wagner, P. M. Winkler, D. R. Worsnop and C. D. O'Dowd, *Atmos. Chem. Phys.*, 2010, **10**, 10561–10605.
18 A. Morita, M. Sugiyama, H. Kameda, S. Koda and D. R. Hanson, *J. Phys. Chem. B*, 2004, **108**, 9111–9120.

19 T. Tsuruta and G. Nagayama, *J. Phys. Chem. B*, 2004, **108**, 1736–1743.
20 J. Vieceli, M. Roeselova and D. J. Tobias, *Chem. Phys. Lett.*, 2004, **393**, 249–255.
21 J. Julin, M. Shiraiwa, R. E. H. Miles, J. P. Reid, U. Pöschl and I. Riipinen, *J. Phys. Chem. A*, 2013, **117**, 410–420.
22 W. S. Drisdell, R. J. Saykally and R. C. Cohen, *J. Phys. Chem. C*, 2010, **114**, 11880–11885.
23 C. D. Cappa, J. D. Smith, W. S. Drisdell and R. J. Saykally, *J. Phys. Chem. C*, 2007, **111**, 7011–7020.
24 A. Nenes, S. Ghan, H. Abdul-Razzak, P. Y. Chuang and J. H. Seinfeld, *Tellus, Ser. B*, 2001, **53**, 133–149.
25 L. M. Russell, S. F. Maria and S. C. B. Myneni, *Geophys. Res. Lett.*, 2002, **29**, 26.
26 H. Tervahattu, J. Juhanoja, V. Vaida, A. F. Tuck, J. V. Niemi, K. Kupiainen, M. Kulmala and H. Vehkamäki, *J. Geophys. Res.: Atmos.*, 2005, **110**, D06207.
27 I. Taraniuk, E. R. Graber, A. Kostinski and Y. Rudich, *Geophys. Res. Lett.*, 2007, **34**, L16807.
28 A. Asa-Awuku, G. J. Engelhart, B. H. Lee, S. N. Pandis and A. Nenes, *Atmos. Chem. Phys.*, 2009, **9**, 795–812.
29 S. Takahama, S. Liu and L. M. Russell, *J. Geophys. Res.: Atmos.*, 2010, **115**, D01202.
30 L. M. Russell, R. Bahadur and P. J. Ziemann, *Proc. Natl. Acad. Sci. U. S. A.*, 2011, **108**, 3516–3521.
31 M. O. Andreae, *Atmos. Chem. Phys.*, 2009, **9**, 543–556.
32 E. Tyrode, C. M. Johnson, S. Baldelli, C. Leygraf and M. W. Rutland, *J. Phys. Chem. B*, 2005, **109**, 329–341.
33 C. M. Johnson, E. Tyrode, S. Baldelli, M. W. Rutland and C. Leygraf, *J. Phys. Chem. B*, 2005, **109**, 321–328.
34 W. S. Drisdell, C. D. Cappa, J. D. Smith, R. J. Saykally and R. C. Cohen, *Atmos. Chem. Phys.*, 2008, **8**, 6699–6706.
35 W. S. Drisdell, R. J. Saykally and R. C. Cohen, *Proc. Natl. Acad. Sci. U. S. A.*, 2009, **106**, 18897–18901.
36 J. D. Smith, C. D. Cappa, K. R. Wilson, R. C. Cohen, P. L. Geissler and R. J. Saykally, *Proc. Natl. Acad. Sci. U. S. A.*, 2005, **102**, 14171–14174.
37 H. Suzuki, Y. Matsuzaki, A. Muraoka and M. Tachikawa, *J. Chem. Phys.*, 2012, **136**, 234508–234514.
38 K. Granados, J. Gracia-Fadrique, A. Amigo and R. Bravo, *J. Chem. Eng. Data*, 2006, **51**, 1356–1360.
39 S. Miyamoto, S. Nakamura, Y. Iwai and Y. Arai, *J. Chem. Eng. Data*, 2001, **46**, 1225–1230.
40 C. Casanova, E. Wilhelm, J.-P. Grolier and H. Kehiaian, *J. Chem. Thermodyn.*, 1981, **13**, 241–248.
41 J. G. Bleazard, T. F. Sun and A. S. Teja, *Int. J. Thermophys.*, 1996, **17**, 111–125.
42 D. M. Murphy and T. Koop, *Q. J. R. Meteorol. Soc.*, 2005, **131**, 1539–1565.
43 R. Hansen, F. Miller and S. Christian, *J. Phys. Chem.*, 1955, **59**, 391–395.
44 E. Psillakis, J. Cheng, M. R. Hoffmann and A. J. Colussi, *J. Phys. Chem. A*, 2009, **113**, 8826–8829.
45 J.-J. Max and C. Chapados, *J. Phys. Chem. A*, 2004, **108**, 3324–3337.
46 P.-A. Bergström, J. Lindgren and O. Kristiansson, *J. Phys. Chem.*, 1991, **95**, 8575–8580.
47 H. Mishra, S. Enami, R. J. Nielsen, L. A. Stewart, M. R. Hoffmann, W. A. Goddard III and A. J. Colussi, *Proc. Natl. Acad. Sci. U. S. A.*, 2012, **109**, 18679–18683.
48 R. J. Saykally, *Nat. Chem.*, 2013, **5**, 82–84.